Reconstruction of solar spectral irradiance since the Maunder minimum

N. A. Krivova,[1] L. E. A. Vieira,[1,2] and S. K. Solanki[1,3]

Received 4 March 2010; revised 1 September 2010; accepted 17 September 2010; published 23 December 2010.

[1] Solar irradiance is the main external driver of the Earth's climate. Whereas the total solar irradiance is the main source of energy input into the climate system, solar UV irradiance exerts control over chemical and physical processes in the Earth's upper atmosphere. The time series of accurate irradiance measurements are, however, relatively short and limit the assessment of the solar contribution to the climate change. Here we reconstruct solar total and spectral irradiance in the range 115–160,000 nm since 1610. The evolution of the solar photospheric magnetic flux, which is a central input to the model, is appraised from the historical record of the sunspot number using a simple but consistent physical model. The model predicts an increase of 1.25 W/m^2, or about 0.09%, in the 11-year averaged solar total irradiance since the Maunder minimum. Also, irradiance in individual spectral intervals has generally increased during the past four centuries, the magnitude of the trend being higher toward shorter wavelengths. In particular, the 11-year averaged Ly-α irradiance has increased by almost 50%. An exception is the spectral interval between about 1500 and 2500 nm, where irradiance has slightly decreased (by about 0.02%).

Citation: Krivova, N. A., L. E. A. Vieira, and S. K. Solanki (2010), Reconstruction of solar spectral irradiance since the Maunder minimum, *J. Geophys. Res.*, *115*, A12112, doi:10.1029/2010JA015431.

1. Introduction

[2] Various observations suggest that the Earth's climate has always been changing. Both internal sources and external drivers contribute to this variability. The most recent strong increase of the global surface temperature appears to be rather unusual, however [*Solomon et al.*, 2007]. Although human activity has been widely recognized to be a major contributor, the relative roles of different drivers are still not well understood and need more accurate evaluation.

[3] The solar radiative output is the main external driver of the Earth's coupled atmospheric and oceanic system [*Hansen*, 2000; *Haigh*, 2001, 2007]. A prime solar quantity for the Earth's climate is solar irradiance, which is the total solar energy flux at the top of the Earth's atmosphere. With the advent of coupled chemistry and general circulation models (GCM), the variability of solar spectral irradiance (SSI) is increasingly coming into the focus of attention of climate research owing to its importance for the chemistry and dynamics of the Earth's atmosphere [*Haigh*, 1994, 2001, 2007; *Langematz et al.*, 2005]. Whereas the total solar irradiance (TSI; i.e., the irradiance integrated over the whole spectrum) changes by about 0.1% between solar activity minimum and maximum [*Fröhlich*, 2006], the UV emission changes by a few percentage points at 200–300 nm to up to 100% around the Ly-alpha emission line near 121.6 nm [*Floyd et al.*, 2003; *Krivova et al.*, 2006]. The variability in the IR is comparable to or lower than the TSI variations. In the range between about 1500 and 2500 nm, i.e., in the vicinity of the atmospheric water vapor absorption bands, the variation over the solar cycle is even reversed with respect to the TSI cycle [*Harder et al.*, 2009; *Krivova et al.*, 2010].

[4] Unfortunately, the time series of accurate measurements of solar and geophysical parameters prior to the increase of manmade greenhouse gases are relatively short, which limits the assessment of the Sun's role in present-day climate change relative to contributions of humanity and to other natural drivers. Reconstructions of these parameters prior to the satellite era are therefore needed to obtain further insight into the nature of solar influence on the Earth's climate on longer time scales.

[5] Recent century-scale reconstructions of the total solar irradiance [*Foster*, 2004; *Lockwood*, 2005; *Wang et al.*, 2005; *Balmaceda et al.*, 2007; *Crouch et al.*, 2008; *Steinhilber et al.*, 2009] suggest that the magnitude of the secular increase in the total irradiance since the Maunder minimum, which was a period of extremely low solar activity observed prior to 1700 [*Eddy*, 1976], is comparable to the solar cycle variation. In most earlier reconstructions, the secular trend was not derived consistently but was *assumed* on the basis of

[1]Max-Planck-Institut für Sonnensystemforschung, Katlenburg-Lindau, Germany.
[2]Laboratory for Physics and Chemistry of the Terrestrial Environment, CNRS, Orleans, France.
[3]School of Space Research, Kyung Hee University, Yongin, South Korea.

0148-0227/10/2010JA015431

solar-stellar comparisons. Such an approach was later criticized, and the derived values, between 2 and 8 W/m^2, were found to be significantly overestimated (for a discussion, see *Krivova et al.* [2007]).

[6] Reconstructions of solar UV irradiance since the Maunder minimum were presented by *Fligge and Solanki* [2000] and *Lean* [2000]. Of these, the first one was based on LTE (local thermodynamic equilibrium) calculations of the solar spectrum, whereas the latter was scaled using UARS/SOLSTICE measurements. The LTE approximation gives inaccurate results below approximately 200 nm and in some spectral lines, whereas the long-term uncertainty of SOLSTICE (indeed, of all instruments that measured solar UV irradiance before SORCE) exceeded the solar cycle variation above approximately 250 nm, thus leading to incorrect estimates of the UV irradiance variability at longer wavelengths (see *Lean et al.* [2005] and *Krivova et al.* [2006]). Furthermore, both reconstructions assumed a higher value of the secular trend than currently accepted as discussed in the previous paragraph.

[7] In this paper, we present a new reconstruction of solar total and spectral irradiance back to the Maunder minimum. It is based on the spectral and total irradiance reconstructions for the telescope era (SATIRE-T) model developed by *Krivova et al.* [2007], which is modified and updated here to take into account the latest observational data and theoretical results. These include the new model of the evolution of solar total and open magnetic flux by *Vieira and Solanki* [2010], the updated reconstruction of the heliospheric magnetic flux by *Lockwood et al.* [2009], the reconstructed solar UV irradiance since 1947 [*Krivova et al.*, 2009a, 2010], and the facular contribution to the TSI variations since 1974 [*Wenzler*, 2005]. Spectral irradiance below 270 nm is calculated following *Krivova et al.* [2006] and *Krivova et al.* [2009a].

[8] The model is described in section 2. The model is validated by computing its output with observed or reconstructed data in section 3. The reconstruction of solar total and spectral irradiance since 1610 is presented in section 4. Section 5 summarizes the results.

2. Model

2.1. SATIRE-T

[9] The current model is a development of the SATIRE-T model presented by *Krivova et al.* [2007]. The SATIRE models [*Solanki et al.*, 2005; *Krivova et al.*, 2010] start from the fundamental assumption that all irradiance variations on time scales longer than a day are caused by the evolution of the solar photospheric magnetic field. This assumption is well supported by the excellent agreement ($r_c^2 > 0.9$) between the calculated irradiance variations and satellite measurements [*Krivova et al.*, 2003; *Wenzler et al.*, 2006]. Visible manifestations of the magnetic field in the solar photosphere are dark sunspots, bright faculae, and the bright network, and they modulate solar brightness. Thus solar irradiance, $F(\lambda, t)$, i.e., the solar radiative flux, at the wavelength λ and the point t in time can be calculated as follows:

$$F(\lambda,t) = \alpha_{\rm q}(t)F_{\rm q}(\lambda) + \alpha_{\rm u}(t)F_{\rm u}(\lambda) + \alpha_{\rm p}(t)F_{\rm p}(\lambda) + [\alpha_{\rm f}(t) + \alpha_{\rm n}(t)]F_{\rm f}(\lambda). \quad (1)$$

Here indices q, u, p, f, and n denote different components of the solar photosphere, namely, the quiet Sun (i.e., solar surface essentially free of magnetic field), sunspot umbra, penumbra as well as faculae, and the network, $F_{\rm i}(\lambda)$ (i = q, u, p, f, n) is the time-independent flux of each component at a given wavelength and $\alpha_{\rm i}(t)$ is the corresponding filling factor at a given time. The spectrum of each component, $F_{\rm i}(\lambda)$, i.e., the flux one would obtain if the whole solar surface were covered by component i, was calculated by *Unruh et al.* [1999] using the ATLAS9 code of *Kurucz* [1993, 2005] from semi-empirical model atmospheres. The same model atmosphere is used here to describe both faculae and the network, i.e., $F_{\rm f} = F_{\rm n}$.

[10] Solar irradiance varies with time because the amount and the distribution of different brightness features (sunspots, faculae, and the network) are steadily changing. This is represented by the so-called filling factors in the model, $\alpha_{\rm i}(t)$. They describe which fraction of the solar surface is covered by each of the photospheric components at a given time. Their assessment is relatively straightforward for the period, when direct measurements of the solar magnetic field (magnetograms) are available. Data of sufficient quality go back to 1974 only [see *Wenzler et al.*, 2006]. At earlier times, no or only lower quality data are available, and the filling factors need to be estimated in a different way. In particular, information on the spatial distribution of the photospheric structures is typically not available for the earlier times. Therefore equation (1) assumes their homogeneous spatial distribution.

2.2. Evolution of the Photospheric Magnetic Flux

[11] *Krivova et al.* [2007] have used the coarse physical model of the evolution of the solar photospheric magnetic flux by *Solanki et al.* [2000, 2002] to compute the filling factors. In this model, all magnetic features on the solar surface are subdivided into active (AR; large bipolar regions emerging in the activity belts and living for up to several weeks) and ephemeral (ER; smaller, short-lived structures emerging at all latitudes) regions. The flux emergence rate in AR and ER is estimated from the historical record of the sunspot number, R_g, as discussed below. Part of the magnetic flux emerging in AR and ER is dragged away from the Sun by the solar wind plasma and reaches far into the heliosphere. This open magnetic flux can survive for several years on the solar surface, since it is often located in large regions with a dominant magnetic polarity. However, some of the flux stays open for a much shorter time, one to several solar rotations [*Ikhsanov and Ivanov*, 1999; *Cranmer*, 2002]. These are possibly smaller, short-lived coronal holes usually associated with a decaying active region. This rapidly decaying open flux component was not taken into account in the original model by *Solanki et al.* [2000, 2002]. *Vieira and Solanki* [2010] have shown, however, that its inclusion significantly improves the agreement between the modeled open flux and its reconstruction based on the aa index.

[12] Thus, four coupled ordinary differential equations describe the evolution of the AR ($\phi_{\rm act}$), ER ($\phi_{\rm eph}$), and of the slow ($\phi^{\rm s}_{\rm open}$) and rapidly ($\phi^{\rm r}_{\rm open}$) decaying open flux

components (for details, see *Vieira and Solanki* [2010]) with time, t:

$$\frac{d\phi_{\rm act}}{dt} = \varepsilon_{\rm act}(t) - \frac{\phi_{\rm act}}{\tau_{\rm act}} - \frac{\phi_{\rm act}}{\tau^{\rm s}_{\rm act}} - \frac{\phi_{\rm act}}{\tau^{\rm r}_{\rm act}}, \quad (2)$$

$$\frac{d\phi_{\rm eph}}{dt} = \varepsilon_{\rm eph}(t) - \frac{\phi_{\rm eph}}{\tau_{\rm eph}} - \frac{\phi_{\rm eph}}{\tau^{\rm s}_{\rm eph}}, \quad (3)$$

$$\frac{d\phi^{\rm s}_{\rm open}}{dt} = \frac{\phi_{\rm act}}{\tau^{\rm s}_{\rm act}} + \frac{\phi_{\rm eph}}{\tau^{\rm s}_{\rm eph}} - \frac{\phi^{\rm s}_{\rm open}}{\tau^{\rm s}_{\rm open}}, \quad (4)$$

$$\frac{d\phi^{\rm r}_{\rm open}}{dt} = \frac{\phi_{\rm act}}{\tau^{\rm r}_{\rm act}} - \frac{\phi^{\rm r}_{\rm open}}{\tau^{\rm r}_{\rm open}}. \quad (5)$$

Note that in the earlier version of the model [*Solanki et al.*, 2002; *Krivova et al.*, 2007], only three equations were considered, without distinguishing between the slow and rapid components of the open flux. The sum of all magnetic field components represents the total photospheric magnetic flux, $\phi_{\rm tot}$:

$$\phi_{\rm tot} = \phi_{\rm act} + \phi_{\rm eph} + \phi^{\rm s}_{\rm open} + \phi^{\rm r}_{\rm open}. \quad (6)$$

[13] In equations (2–5), $\tau_{\rm act}$, $\tau_{\rm eph}$, $\tau^{\rm s}_{\rm open}$ and $\tau^{\rm r}_{\rm open}$ are the decay time scales for AR, ER, and slow and rapid components of the open flux, respectively, whereas $\tau^{\rm s}_{\rm act}$, $\tau^{\rm s}_{\rm eph}$ and $\tau^{\rm r}_{\rm act}$ are the flux transfer times from active and ephemeral regions to the slow and rapid open magnetic flux. Of these seven parameters, $\tau_{\rm eph}$ is fixed to 14 h (or 0.0016 yr) according to observations by *Hagenaar* [2001]. All others are left free within the limits provided by appropriate observations, as discussed by *Krivova et al.* [2007] and *Vieira and Solanki* [2010] (see also Table 1).

[14] The flux emergence rates of AR, $\varepsilon_{\rm act}$, and ER, $\varepsilon_{\rm eph}$, which are the main inputs to the model, are calculated from the historical group sunspot number, R_g [*Hoyt and Schatten*, 1993]. The emergence rate in active regions, $\varepsilon_{\rm act}$, is taken to be linearly proportional to the sunspot number and is scaled according to the observations of *Schrijver and Harvey* [1994] for cycle 21. ER cycle is extended with respect to the AR cycle (see, e.g., *Harvey* [1992, 1993, 1994]), and its length and amplitude are assumed to be related to the properties of the corresponding sunspot cycle. The latter is justified if ER are produced by the same dynamo mechanism as the AR. This introduces two additional free parameters into the model: the scaling factor X between the emergence rates of ER, $\varepsilon_{\rm eph}$, and AR, $\varepsilon_{\rm act}$, and the ER cycle length extension parameter, c_x (see *Krivova et al.* [2007] and *Vieira and Solanki* [2010] for further details).

2.3. Filling Factors

[15] After the magnetic flux is calculated as described above, the filling factors $\alpha_{\rm i}$ needed to calculate solar irradiance (see equation (1)) can be derived.

[16] The filling factors for sunspots are calculated directly from the sunspot areas since 1874 [*Balmaceda et al.*, 2009]. Before 1874, a correlation analysis between sunspot areas and numbers is first carried out to compute sunspot areas for that earlier period. Following *Krivova et al.* [2007], we employ a fixed ratio between umbral and penumbral areas, $\alpha_{\rm u}/(\alpha_{\rm u} + \alpha_{\rm p}) = 0.2$ [*Brandt et al.*, 1990; *Solanki*, 2003; *Wenzler*, 2005].

[17] The filling factors of faculae and the network are calculated from the corresponding modeled magnetic fluxes. The sum of the ER and open magnetic fluxes represents the evolution of the network: $\phi_{\rm n} = \phi_{\rm eph} + \phi_{\rm open}$. Facular magnetic flux, $\phi_{\rm f}$, is derived from the AR magnetic flux after subtraction of the magnetic flux of sunspots: $\phi_{\rm f} = \phi_{\rm act} - \phi_{\rm s}$. The latter, $\phi_{\rm s}$, is the product of sunspot area and the mean magnetic field strength in sunspots [see *Krivova et al.*, 2007]. To convert magnetic fluxes into filling factors, we apply the same scheme as in all SATIRE models [e.g., *Krivova et al.*, 2003; *Wenzler et al.*, 2006; *Krivova et al.*, 2007]: the filling factors $\alpha_{\rm f}$ and $\alpha_{\rm n}$ are proportional to the corresponding magnetic fluxes, $\phi_{\rm f}$ and $\phi_{\rm n}$, until a saturation limit, $\phi_{\rm sat,f}$ and $\phi_{\rm sat,n}$, is reached. Above the corresponding saturation limits are $\alpha_{\rm f} = 1$ and $\alpha_{\rm n} = 1$. The value of $\phi_{\rm sat,n}$ is fixed to 800 G, in agreement with the results obtained for the model based on magnetograms [*Krivova et al.*, 2007]. Note that these 800 G correspond to the value of 500 G employed by *Krivova et al.* [2007] for the newer calibration of the MDI magnetograms [*Tran et al.*, 2005] (*Krivova et al.* still employed the older calibration). The saturation limit for faculae, $\phi_{\rm sat,f}$, is left free.

[18] Finally, the area not covered by photospheric magnetic structures (sunspots, faculae, and network elements) is considered to be the quiet Sun: $\alpha_{\rm q} = 1 - \alpha_{\rm u} - \alpha_{\rm p} - \alpha_{\rm f} - \alpha_{\rm n}$.

2.4. Parameters and Optimization

[19] Our model thus has nine free parameters, summarized in Table 1, i.e., one more than in the magnetic flux model by *Vieira and Solanki* [2010]. The additional parameter, $\phi_{\rm sat,f}$, is the only one that is directly related to the irradiance reconstructions (as in all SATIRE models), i.e., to the conversion of the magnetic flux into irradiance. To constrain the free parameters as tightly as possible, we compare the model results with different sets of available observational data or with other models, i.e., we require that the modeled time series simultaneously match as well as possible five distinct related independent records.

[20] Following *Vieira and Solanki* [2010], the modeled total magnetic flux is confronted with the measurements carried out at the Mt. Wilson Solar Observatory (MWO), National Solar Observatory Kitt Peak (KP NSO), and Wilcox Solar Observatory (WSO) over cycles 20–23 [*Arge et al.*, 2002; *Wang et al.*, 2005]. The calculated open magnetic flux is compared to the reconstruction by *Lockwood et al.* [2009] since 1904. Following *Krivova et al.* [2007], we also require the computed TSI variations to match the PMOD composite of space-based measurements since 1978 [*Fröhlich*, 2005, 2008; version d41_62_0906].

[21] Here we have also added two new records to constrain the model further. These are (1) the facular contribution to the TSI variations over 1978–2003, computed by *Wenzler* [2005] with the SATIRE-S model from KP NSO magnetograms and continuum images; and (2) the solar irradiance flux integrated over wavelengths 220–240 nm over the period 1947–2006 as reconstructed by *Krivova et al.* [2009a] and *Krivova et al.* [2010] using solar F10.7 cm radio flux (before 1974) and KP NSO as well as MDI

Table 1. Parameters of the Model Providing the Best Fit to the Five Considered Data Sets and Their Allowed Ranges[a]

Parameter	Notation	Value	Min	Max
AR decay time	τ_{act}	0.30	0.2	0.8
ER decay time	τ_{eph}	0.0016	Fixed	
Slow OF decay time	τ^{s}_{open}	2.97	0.0016	6.0
Rapid OF decay time	τ^{r}_{open}	0.16	0.08	0.36
AR to slow OF transfer time	τ^{s}_{act}	71.2	10	90
AR to rapid OF transfer time	τ^{r}_{act}	2.1	0.0016	3.0
ER to slow OF transfer time	τ^{s}_{eph}	17.8	10	90
ER cycle amplitude factor	X	78	70	150
ER cycle extension	c_x	5.01	5	9
Saturation flux in faculae, G	$\phi_{sat,f}$	156.1	50	850
Saturation flux in network, G	$\phi_{sat,n}$	800	Fixed	

[a]Times are given in years.

magnetograms and continuum images (after 1974). The two new sets serve, first, to provide further constraints on the model and the values of the free parameters. Second, they ensure that not only the total (integrated over all wavelengths) irradiance is reproduced correctly but also its spectral distribution. The contribution of the UV wavelengths to the total irradiance is relatively weak (less than 8% for all wavelengths below 400 nm; *Krivova et al.* [2006]), and thus errors in its calculation are not necessarily evident in the TSI. Also, since faculae dominate irradiance variations in the UV [e.g., *Unruh et al.*, 2008], it is crucial that their evolution is modeled properly. Thus, although we now have one free parameter more than in the model by *Vieira and Solanki* [2010], the model is required to reproduce three additional independent records and is therefore better constrained.

[22] Following *Krivova et al.* [2007] and *Vieira and Solanki* [2010], we utilize the PIKAIA optimization routine [http://www.hao.ucar.edu; *Charbonneau*, 1995] to minimize the mean of the χ^2 values (weighted by the degrees of freedom) between the five modeled and corresponding measured (or independently reconstructed) time series. Further details are given in previous papers [*Krivova et al.*, 2007; *Vieira and Solanki*, 2010].

3. Validation of the Model

[23] Here we first consider how well our model agrees with the five independent time series used to constrain the model parameters as outlined in section 2. The best estimates of the free parameters are listed in Table 1. Figure 1a shows the total magnetic flux between 1967 and 2007 (solid line). The total flux displayed there is calculated as $\phi_{act} + 0.3\phi_{eph} + \phi_{open}$. The factor 0.3 for the ER component takes into account the finding of *Krivova and Solanki* [2004] that more than half of the ER magnetic flux remains undetected in the harnessed synoptic charts owing to insufficient spatial resolution. Also plotted are the measurements by KP NSO (squares), MWO (diamonds), and WSO (triangles). Each data point is an integral over a synoptic chart for one Carrington rotation. Note that for the optimization, only the period between 1974 and 2002 is used, when all three observatories performed observations. The model is plotted against the measurements in Figure 1b. The solid line in this figure represents the linear regression fit to the data, with a slope of 1.06, whereas the dashed line depicts the ideal fit (with a slope of 1). The correlation coefficient between the model and the observations is $R_c = 0.93$.

[24] The results for the open magnetic flux are displayed in Figure 2. Figure 2a shows the time series of the modeled open flux since 1900 and of the independent reconstruction by *Lockwood et al.* [2009] from the geomagnetic aa index, whereas Figure 2b confronts one with the other directly. The correlation coefficient between the two is 0.86.

[25] Another test of the calculated open flux is offered by its comparison with the cosmogenic isotope data. Their production rate depends on the galactic cosmic ray flux, which is modulated by the solar open magnetic flux. *Usoskin et al.* [2006], in particular, demonstrated that being independent of terrestrial processes, the activity of cosmogenic isotope ^{44}Ti in meteorites represents a good proxy of secular variations of solar open magnetic flux. The activity of the cosmogenic isotope ^{44}Ti calculated from our reconstructed open flux (I. Usoskin, personal communication, 2010) is found to be in good agreement with the measurements.

[26] Figure 3 displays changes in the TSI over cycles 21–23. The model is represented by the dotted line, and the PMOD composite of measurements [*Fröhlich*, 2005, 2006, 2008] is indicated by the solid line. The correlation coefficient between the daily time series is 0.81, which is slightly higher

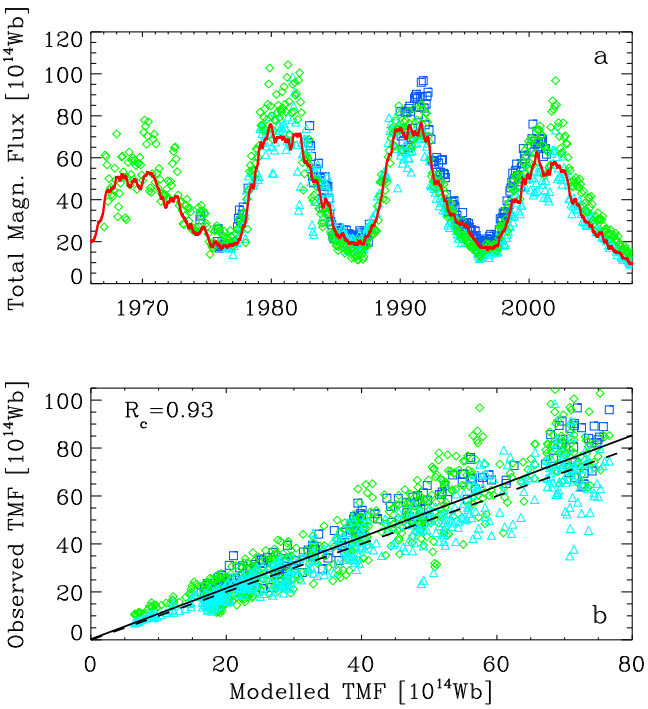

Figure 1. (a) Measured (symbols) and modeled (solid line) total magnetic flux since 1967. Each data point is an integral over a synoptic chart of one Carrington rotation. Different symbols are used for different data sets: KP NSO (squares), MWO (diamonds) and WSO (triangles). For the modelled flux, the value $\phi_{act} + 0.3\phi_{eph} + \phi_{open}$ is given. (b) Measured total magnetic flux versus modeled. The solid line represents the linear regression fit ($R_c = 0.93$; slope is 1.06), and the dashed line represents the expectation values, i.e., an ideal fit (with a slope of 1).

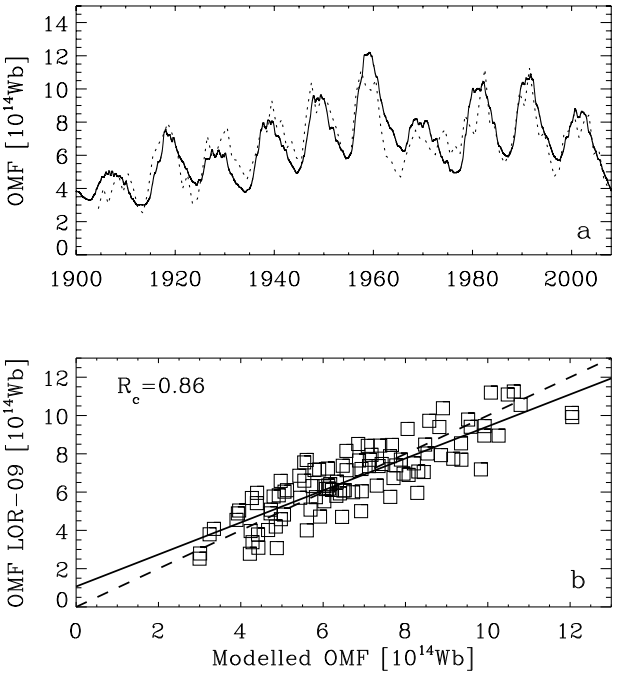

Figure 2. (a) Evolution of the modeled (yearly averages; solid line) open magnetic flux since 1900 compared to the reconstruction by *Lockwood et al.* [2009] since 1904 based on the geomagnetic aa index (dotted line). (b) Open magnetic flux from *Lockwood et al.* [2009] versus modeled. The solid line represents the linear regression fit (R_c = 0.86, slope is 0.84), and the dashed line represents the ideal fit.

than in the previous version of the model [0.79; *Krivova et al.*, 2007]. As discussed by *Vieira and Solanki* [2010], owing to the extended length of the ER cycle, around activity minima both the preceding and following cycles contribute to the magnetic flux (and thus irradiance). Since the features of the next cycle (24) are not yet known and we wanted to avoid any speculations, we neglected this cycle and did not take the declining phase of cycle 23 into account in the optimization. The missing cycle 24 leads to obviously too low values of TSI for the current minimum. Thus irradiance values after around 2005 are unreliable. For this reason also, the current model cannot be used to test the claim of *Fröhlich* [2009] that the lower level of the TSI during the current minimum compared to the previous one is of nonmagnetic origin. This question will be addressed separately in a forthcoming paper (Vieira et al., manuscript in preparation), where the unknown strength and length of cycle 24 are introduced into the model as additional free parameters, leading to a good agreement also with TSI values of the current minimum.

[27] Another feature of the model is that the true shape of the cycle cannot be reproduced with high precision. The reason is the lack of detailed information on the emergence rate of the magnetic flux in bright magnetic features (faculae and the network) responsible for the Sun's brightening during activity maxima. In the model, they are assumed to be related to the evolution of sunspots, which is a reasonable assumption on time scales of multiple months and longer, but does not necessarily hold on time scales of days to months (see paper by *Preminger and Walton* [2005] showing that spots and faculae are offset in time relative to each other). Thus the evolution of the facular and network components cannot be recovered on a daily basis. Note that the dips in the irradiance, which are caused by sunspots, are still well replicated, since they are described by real sunspot area observations. Thus caution should be exercised when using this model for analysis of irradiance trends on time scales of several weeks to about 1–2 years [cf. *Krivova et al.*, 2009b]. This peculiarity is also seen in Figure 3b, where the difference between the model and the PMOD composite of measurements is plotted. For the reasons mentioned above,

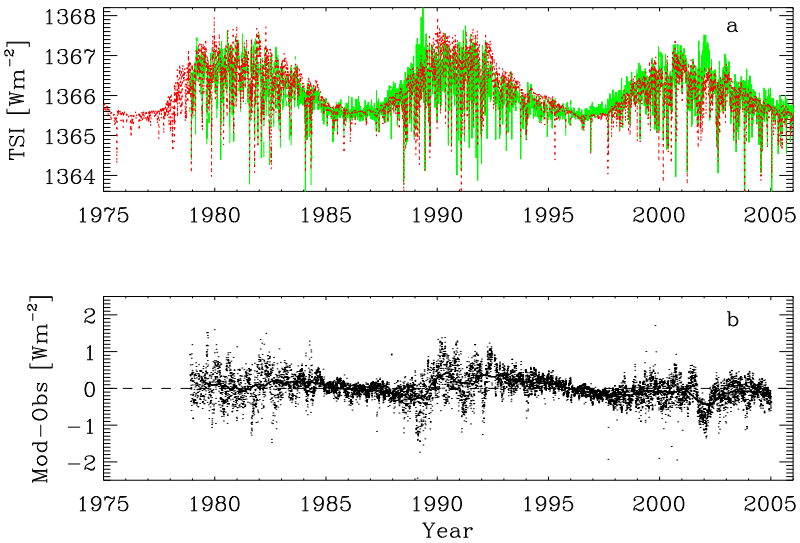

Figure 3. (a) Modeled (dotted line) and measured (PMOD composite, solid line) daily total solar irradiance over cycles 21–23. (b) Difference between the modeled and measured (PMOD composite) TSI. Dots represent daily values, and the solid line represent the values smoothed over 1 year.

we do not plot the period after 2005. Although when averaged over the whole period this difference is clustered around 0 with no evident long-term trend, the difference shows some systematic trends during a cycle. Thus both the rise and the decline in the modeled irradiance are typically slightly delayed compared to the observations, i.e., the cycles are more symmetric in the model than in reality. This systematic difference in the cycle shape also leads to the relatively low value of the linear regression slope between the modeled and observed TSI (Table 2).

[28] Since the main goal of this work is a reconstruction of the solar spectral irradiance over the past four centuries, it is important to validate the model against data, which are particularly sensitive to the correct representation of the solar spectral energy distribution, in particular in the UV. We found two such sets: the facular contribution to the TSI variations deduced by *Wenzler* [2005] from the KP NSO magnetograms and continuum images and solar irradiance integrated over the wavelength range 220–240 nm calculated by *Krivova et al.* [2009a, 2010] from the solar F10.7 cm radio flux (before 1974, proxy model) and NSO KP and MDI magnetograms and continuum images (after 1974, SATIRE-S). For the period since 1996, the values computed by *Krivova et al.* [2009a, 2010] are in excellent agreement with SUSIM measurements. Hence the quantities we are comparing are finally anchored in measurements.

[29] The modeled facular contribution to the TSI variability and the 220–240 nm radiative flux are shown and compared to the corresponding independent series in Figures 4 and 5, respectively. As discussed above, our model is not expected to give accurate results for facular and network evolution (and thus also UV irradiance) on time scales shorter than a few months. Therefore, the comparison (as well as the optimization) was performed for these two records after smoothing over 3 months.

[30] Figures 4a and 5a show the time series, both modeled here (solid lines) and deduced previously by independent means (dashed lines). Figures 4b and 5b compare each of the sets with the appropriate independent record. The correlation coefficients are 0.94 in both cases.

[31] Table 2 summarizes the main quantities reflecting the agreement between the modeled time series and the corresponding measurements or independent reconstructions. Listed are the shortest time scales, on which the data were compared (the longest time scale corresponds to the length of the observed data set), the correlation coefficients, slopes of the linear regressions, and χ^2 values. For the total and open magnetic flux, also the χ^2 values obtained for the model by *Vieira and Solanki* [2010] are indicated. They are slightly lower than the values obtained here, which is not surprising. As mentioned by *Vieira and Solanki* [2010], the set of parameters obtained by them is not unique, and similarly good fits can be reached with somewhat different values. This is partly because some of the parameters are not absolutely independent and have similar effects on the results. Since here we required the model to fit three additional data sets, this constrains the free parameters further, and thus it is not unexpected that fits to the individual data sets can be somewhat worse. In fact, it is rather encouraging that we still obtain fits of essentially the same quality ($\chi^2 = 0.069$ and 0.248 compared to 0.065 and 0.222 from *Vieira and Solanki* [2010] for the total and open flux, respectively; Table 2). Further discussion on the magnetic flux evolution, including contributions of different components (AR, ER, and open flux) can be found in the paper by *Vieira and Solanki* [2010].

[32] Yet another test of the quality of the model is offered by a comparison of the reconstructed solar irradiance in Ly-α line with available measurements and a proxy model. Since this quantity was not taken into account in the optimization and a comparison was carried out a posteriori, this is discussed in section 4.

4. Irradiance Reconstruction

4.1. Total Solar Irradiance

[33] Figure 6 shows the reconstructed TSI since 1610. The thin solid line represents daily values, and the thick line represents the values after 11-year smoothing. Also shown are the measurements available since 1978 (shaded dots). Between the end of the 17th century (i.e., the end of the Maunder minimum) and the end of the 20th century (represented as an average over 1975–2005), the TSI has increased by 1.25 W/m^2, or about 0.09%. This is in good agreement with the earlier estimates by *Balmaceda et al.* [2007] and *Krivova et al.* [2007], who obtained a value of 1.3 W/m^2. This good agreement of the new version of the model presented here, which involves a more accurate representation of the open magnetic flux evolution and uses two additional data sets (facular contribution to the TSI variation and irradiance at 220–240 nm) to constrain the model's free parameters, is an encouraging result.

[34] This suggests that the model is rather tolerant to some unavoidable assumptions and uncertainty in the values of the free parameters (see also discussion of errors in *Vieira and Solanki* [2010]). Even for two extreme assumptions, time-independent ER flux and ER cycles being in antiphase with AR cycles, *Krivova et al.* [2007] obtained values of about 1.5 W/m^2 and 0.9 W/m^2 for the increase since the Maunder minimum, respectively. All these values thus lie within a rather tightly confined range, also consistent with the results obtained by other methods [e.g., *Foster*, 2004; *Lockwood*, 2005; *Wang et al.*, 2005; *Steinhilber et al.*, 2009].

4.2. Solar Spectral Irradiance

[35] By design, SATIRE models allow reconstruction of both total and spectral solar irradiance (see section 2.1 and equation (1)). However, since the local thermodynamic equilibrium (LTE) approximation is involved in calculations of brightness spectra of different surface features (section 2.1) from the appropriate model atmospheres [see also *Unruh et al.*, 1999], which is expected to fail in the UV, the irradiance below about 200 nm and in some stronger lines above 200 nm is not reliable.

[36] *Krivova et al.* [2006, 2009a] have found that, despite the LTE approximation, SATIRE models work well in the spectral range 220–240 nm, as well as at the wavelengths above approximately 270 nm. To extend the model to other wavelengths below 270 nm, which are of special interest for climate studies, they worked out a technique that makes use of the available measurements of solar irradiance in the UV by the UARS/SUSIM instrument. Empirical relationships have been constructed between the irradiance in the range 220–240 nm and irradiances at other wavelengths between 115 and 270 nm. Thus, whenever irradiance at 220–240 is

Table 2. Parameters Quantifying the Quality of Fits Between the Modeled and Corresponding Independent Time Series[a]

Quantity	t Scale	R_c	Slope	χ^2	χ^2–VS10
Total magnetic flux	1 CR[b]	0.93	1.06 ± 0.01	0.069	0.065
Open magnetic flux	1 yr	0.86	0.84 ± 0.05	0.248	0.222
TSI	1 day	0.81	0.76 ± 0.01	0.233	-
Facular contribution to TSI variation	3 months	0.94	0.94 ± 0.004	0.064	-
UV flux (220–240 nm)	3 months	0.94	0.99 ± 0.003	0.072	-

[a]Listed are quantity that has been compared, time scale on which the comparison was performed, the correlation coefficient, R_c, the slope of the linear regression, χ^2 between the time series under examination, and χ^2 obtained by *Vieira and Solanki* [2010] if available (χ^2–VS10).
[b]CR, Carrington rotation.

available, it is also possible to reconstruct irradiance over the whole range 115–270 nm. We have applied this technique here to also calculate the spectral irradiance over the range 115–270 nm.

[37] The quality of this reconstruction can be judged from a comparison of the modeled irradiance in Ly-α line with available measurements by UARS/SUSIM between 1991 and 2005 and a composite time series compiled by *Woods et al.* [2000]. The composite comprises the measurements

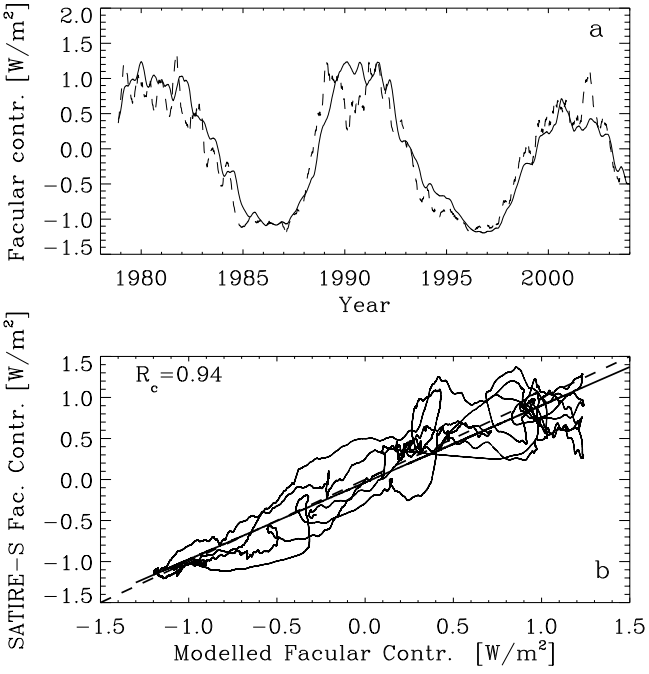

Figure 4. (a) Facular contribution to the TSI variation calculated in this work (solid line) and using KP NSO magnetograms and continuum images (SATIRE-S; dashed line) [*Wenzler et al.*, 2006]. Plotted are the 3-month running means of the variation around mean values. (b) Facular contribution to the TSI from the SATIRE-S model versus the one calculated here. The solid line represents the linear regression fit (R_c = 0.94, slope is 0.94), and the dashed line represents the ideal fit.

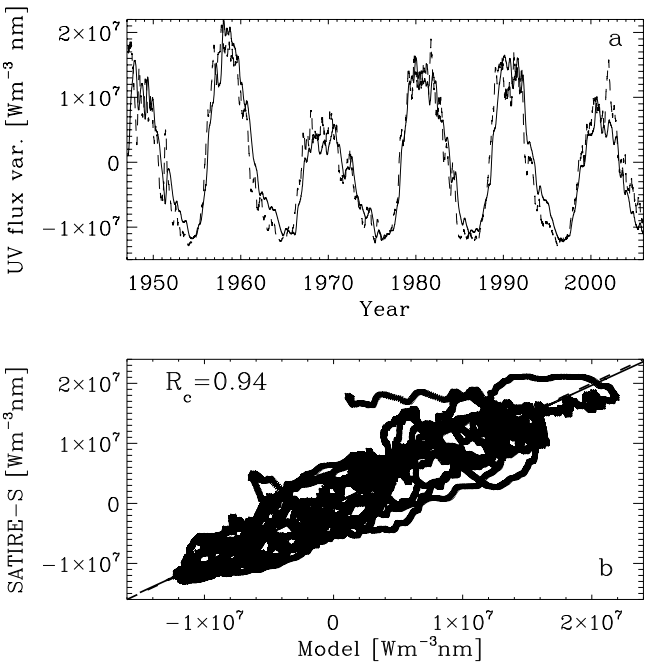

Figure 5. (a) Solar radiative flux integrated over the wavelength range 220–240 nm (3-month running means). The dashed line shows the SATIRE-S reconstruction based on the solar F10.7 radio flux (before 1974) as well as on the KP NSO and MDI magnetograms and continuum images [*Krivova et al.*, 2009a, 2010]. The solid line shows the model presented here. (b) Solar 220–240 nm flux from the independent SATIRE-S reconstruction versus the model presented here. The solid line represents the linear regression fit (R_c = 0.94, slope is 0.99), and the dashed line represents the ideal fit.

from the Atmospheric Explorer E (AE-E; 1977–1980), the Solar Mesosphere Explorer (SME; 1981–1989), UARS SOLSTICE (1991–2001), and the Solar EUV Experiment (SEE) on TIMED (Thermosphere, Ionosphere, Mesosphere Energetics and Dynamic Mission launched in 2001). The gaps are filled in using proxy models on the basis of Mg core-to-wing and F10.7 indices, and the F10.7 model is also used to extrapolate the data set back in time. All three series are plotted in Figure 7, with Figures 7a and 7b showing daily and 3-month smoothed data, respectively. The model is represented by the red line, SUSIM data by the green line, and the composite record by the blue line. As in the case of the TSI, owing to the missing ephemeral regions from cycle 24, the model gives too low Ly-α irradiance values from roughly 2005 onward, so that we stop comparing its output with the data around then. By the model design, the magnitude of the solar cycle variation agrees better with the SUSIM data than with the composite [see *Krivova et al.*, 2009a]. The correlation coefficients are 0.85 between the daily sampled model and the SUSIM data and 0.89 between the model and the composite record. For the 3-month smoothed records, the correlation between the model and the composite by *Woods et al.* [2000] is 0.95. Note, however, that as discussed in section 3, the shape of the cycles cannot be reproduced very accurately by the model design, so that times of activity minima and maxima may differ

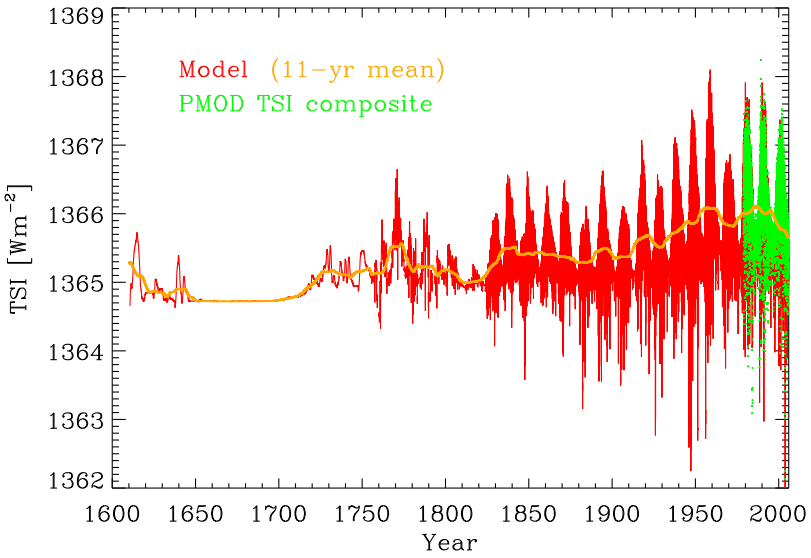

Figure 6. Reconstructed solar total irradiance since 1610 (thin solid line). Also shown are the 11-year smoothed TSI (thick solid line) and PMOD composite of measurements since 1978 (shaded dots).

from the real ones by about 1–2 years. A complete Ly-α time series since 1610 is displayed in Figure 8. Averaged over 11 years, Ly-α irradiance has increased by almost 50% since the end of the Maunder minimum.

[38] Figure 9 shows the reconstructed irradiance integrated over some spectral ranges of particular interest for climate studies: Figure 9a shows the Schumann-Runge oxygen continuum, 130–175 nm; Figure 9b shows the Schumann-Runge oxygen bands, 175–200 nm; Figure 9c shows the Herzberg oxygen continuum, 200–242 nm; Figure 9d shows the Hartley-Huggins bands, 200–350 nm; and Figures 9e and 9f show two IR intervals containing water vapor absorption bands of 800–1500 nm and 1500–2500 nm, respectively. The variability is significantly stronger at shorter wavelengths, as previously found for solar cycle time scales [*Floyd et al.*, 2003; *Krivova et al.*, 2009a, 2010], and in the range between around 1500–2500 nm it is reversed compared to other wavelengths. The inverse solar cycle variability in this

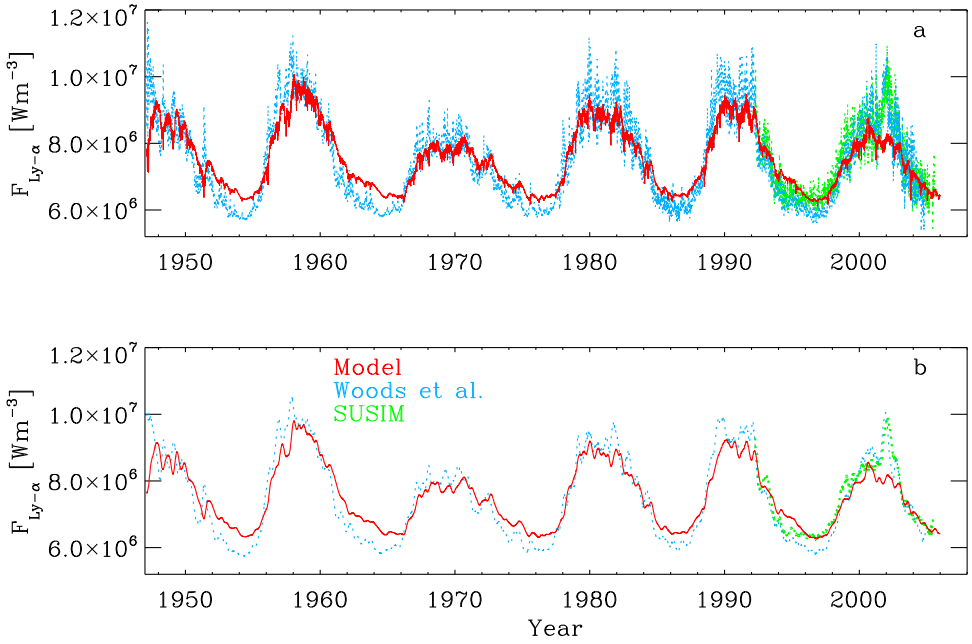

Figure 7. (a) Daily reconstructed irradiance in Ly-α (red line) since 1947. Also shown are SUSIM measurements (green) and the composite (blue) of measurements and proxy models by *Woods et al.* [2000]. The correlation coefficients are 0.85 and 0.89 between the model and the SUSIM data and between the model and the composite, respectively. (b) Same as Figure 7a, but for 3-month running means.

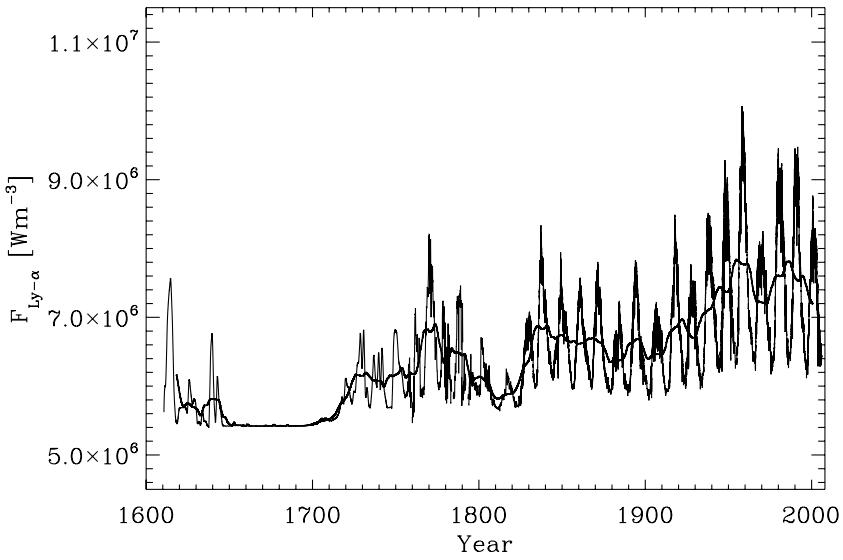

Figure 8. Reconstructed solar irradiance in Ly-α: daily (thin solid line) and smoothed over 11 years (thick line).

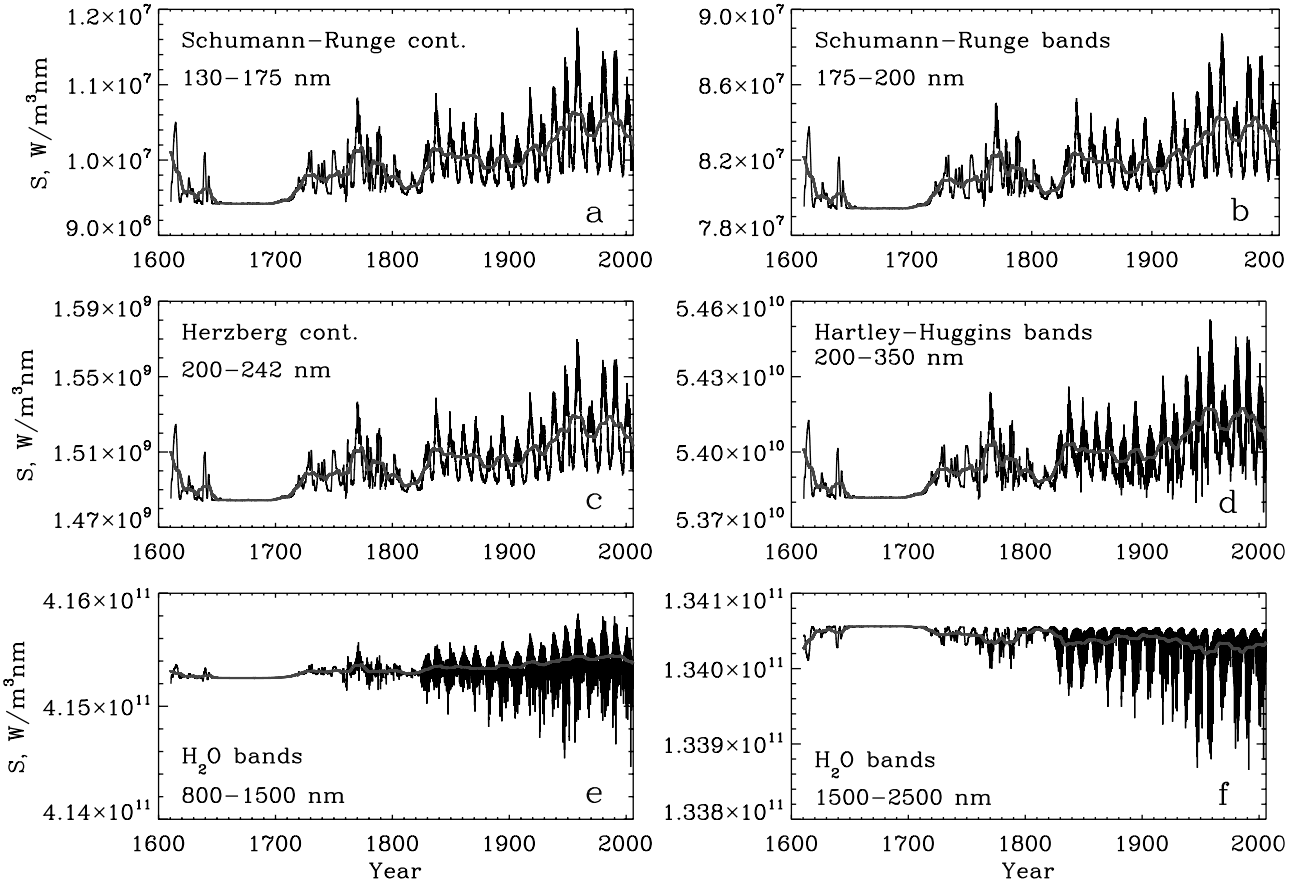

Figure 9. Reconstructed solar irradiance in selected spectral intervals of special interest for climate models: daily (thin lines) and smoothed over 11 years (thick lines). (a) Shumann-Runge oxygen continuum. (b) Schumann-Runge oxygen bands. (c) Herzberg oxygen continuum. (d) Hartley-Huggins ozone bands. (e and f) Water vapor infrared bands. The exact wavelength ranges are indicated in each part.

range has previously been noted by *Harder et al.* [2009] on the basis of SORCE/SIM observations in cycle 23 and by *Krivova et al.* [2010] on the basis of the SATIRE-S model results. This is explained by the low or even negative contrast of faculae at these wavelengths [*Unruh et al.*, 2008], so that their brightening (if any) no longer compensates the darkening due to sunspots. The increased amount of the facular and ER surface coverage since the Maunder minimum (as a result of the increase in the corresponding magnetic fluxes (see *Vieira and Solanki* [2010]) thus also leads to an overall decrease (of the order of 0.02%) in the irradiance at 1500–2500 nm.

[39] The complete time series of the reconstructed spectral and total irradiance are available from http://www.mps.mpg.de/projects/sun-climate/data.html.

5. Summary

[40] Solar irradiance has long been recognized as an important climate driver [*Hansen*, 2000; *Haigh*, 2001, 2007]. Nonetheless, the main processes through which the Sun affects global climate remain uncertain. Whereas the total solar irradiance is the main external source of energy entering the Earth's climate system, solar UV irradiance governs chemical and physical processes in the Earth's upper atmosphere.

[41] Accurate assessment of the solar forcing on the Earth's climate is partly hampered by a shortage of reliable and sufficiently long irradiance records. Although significant attention has been paid in recent years to reconstructions of solar total irradiance, long-term reconstructions of solar spectral irradiance [*Fligge and Solanki*, 2000; *Lean*, 2000] suffered from the fact that they estimated the magnitude of the long-term trend from stellar data that have in the meantime been refuted. The SATIRE set of models [*Solanki et al.*, 2005; *Krivova et al.*, 2010] provide a tool to reconstruct solar total *and* spectral irradiance. However, since the LTE approximation underlies the computations of the brightness spectra of different photospheric components, the original version of the model fails in the UV. Although it contributes little to the total irradiance (such that the modeled TSI is nevertheless quite accurate), this wavelegth range on its own is of special interest for climate research owing to its important influence on the chemistry and dynamics of the Earth's atmosphere [*Haigh*, 1994, 2007; *Langematz et al.*, 2005].

[42] The most recent empirical extension of the SATIRE models to shorter wavelengths [*Krivova et al.*, 2006, 2009a] makes it possible to reconstruct solar spectral irradiance over a broad spectral range between 115 nm and 160 μm. Here we combined this empirical technique with the SATIRE-T model previously used by *Balmaceda et al.* [2007] and *Krivova et al.* [2007] to reconstruct solar total irradiance since the Maunder minimum. In the SATIRE-T model, the sunspot number and, whenever available, sunspot areas are used to reconstruct the evolution of the solar surface magnetic field following *Solanki et al.* [2000, 2002], which is then converted into irradiance. Recently, the physical model of the solar photospheric magnetic field was reconsidered and updated by *Vieira and Solanki* [2010], so that it now provides an even better agreement with the independent open flux reconstruction from the geomagnetic aa index [*Lockwood et al.*, 2009].

[43] We have used this improvement to first update the reconstruction of the TSI since 1610. The new reconstruction shows a slightly better agreement with the PMOD composite of TSI measurements (with a linear correlation coefficient of 0.81 compared to 0.79) than the earlier version, although the two versions are still consistent with each other. We now find a value of about 1.25 W/m^2 as our best estimate for the 11-year averaged increase in the TSI between the end of the Maunder minimum and the end of the 20th century, compared to 1.3 W/m^2 derived by *Balmaceda et al.* [2007] and *Krivova et al.* [2007].

[44] We have then combined the SATIRE-T model with the empirical extension of the model to shorter wavelengths and calculated solar spectral irradiance for the past 400 years over the spectral range 115 nm to 160 μm. We required the model to fit two additional independent time series, namely, the facular contribution to the TSI variation and the solar UV flux over the range 220–240 nm as derived with the SATIRE-S model on the basis of KP NSO and MDI magnetograms and continuum images [*Wenzler*, 2005; *Wenzler et al.*, 2006; *Krivova et al.*, 2009a]. This allowed better constraints to be set on the model's free parameter and put a special emphasis on the correct replication of the spectral distribution of the irradiance.

[45] Thus the main result of this work is a reconstruction of solar total and spectral irradiance over a broad range between 115 nm and 160 μm since 1610. This fully covers the range of interest for the state-of-the-art climate models. The data set is available online at http://www.mps.mpg.de/projects/sun-climate/data.html.

[46] **Acknowledgments.** The composite Lyman α time series was retrieved from the LASP ftp server (laspftp.colorado.edu). This work was supported by the Deutsche Forschungsgemeinschaft, DFG project SO 711/1-2 and by WCU grant R31-10016 funded by the Korean Ministry of Education, Science and Technology. We thank the International Space Science Institute (Bern) for hosting the meetings of the international team on "Interpretation and modeling of SSI measurements." LEAV acknowledges support by the European Commission's Seventh Framework Programme (FP7/2007–2013; grant 218816).

[47] Philippa Browning thanks the reviewers for their assistance in evaluating this paper.

References

Arge, C. N., E. Hildner, V. J. Pizzo, and J. W. Harvey (2002), Two solar cycles of nonincreasing magnetic flux, *J. Geophys. Res.*, *107*(A10), 1319, doi:10.1029/2001JA000503.

Balmaceda, L., N. A. Krivova, and S. K. Solanki (2007), Reconstruction of solar irradiance using the Group sunspot number, *Adv. Space Res.*, *40*, 986–989.

Balmaceda, L. A., S. K. Solanki, N. A. Krivova, and S. Foster (2009), A homogeneous sunspot areas database covering more than 130 years, *J. Geophys. Res.*, *114*, A07104, doi:10.1029/2009JA014299.

Brandt, P. N., W. Schmidt, and M. Steinegger (1990), On the umbra-penumbra area ratio of sunspots, *Solar Phys.*, *129*, 191–194.

Charbonneau, P. (1995), Genetic algorithms in astronomy and astrophysics, *Astrophys. J. Suppl. Ser.*, *101*, 309–334.

Cranmer, S. R. (2002), Coronal holes and the high-speed solar wind, *Space Sci. Rev.*, *101*, 229–294.

Crouch, A. D., P. Charbonneau, G. Beaubien, and D. Paquin-Ricard (2008), A model for the total solar irradiance based on active region decay, *Astrophys. J.*, *677*, 723–741, doi:10.1086/527433.

Eddy, J. A. (1976), The Maunder minimum, *Science*, *192*, 1189–1202.

Fligge, M., and S. K. Solanki (2000), The solar spectral irradiance since 1700, *Geophys. Res. Lett.*, *27*, 2157–2160, doi:10.1029/2000GL000067.

Floyd, L., G. Rottman, M. DeLand, and J. Pap (2003), 11 years of solar UV irradiance measurements from UARS, *ESA SP*, *535*, 195–203.

Foster, S. (2004), Reconstruction of solar irradiance variations for use in studies of global climate change: Application of recent SOHO observations with historic data from the Greenwich observatory, Ph.D. thesis, University of Southhampton, School of Physics and Astronomy.

Fröhlich, C. (2005), Solar irradiance variability since 1978, *Mem. Soc. Astron. It.*, *76*, 731–734.
Fröhlich, C. (2006), Solar irradiance variability since 1978: Revision of the PMOD composite during solar cycle 21, *Space Sci. Rev.*, *125*, 53–65.
Fröhlich, C. (2008), Total solar irradiance variability: What have we learned about its variability from the record of the last three solar cycles?, in *Climate and Weather of the Sun-Earth System (CAWSES): Selected Papers from the 2007 Kyoto Symposium*, edited by T. Tsuda et al., pp. 217–230, Terra Publishing, Setagaya-ku, Tokyo, Japan.
Fröhlich, C. (2009), Evidence of a long-term trend in total solar irradiance, *Astron. Astrophys.*, *501*, L27–L30.
Hagenaar, H. J. (2001), Ephemeral regions on a sequence of full-disk Michelson Doppler Imager magnetograms, *Astrophys. J.*, *555*, 448–461.
Haigh, J. D. (1994), The role of stratospheric ozone in modulating the solar radiative forcing of climate, *Nature*, *370*, 544–546.
Haigh, J. D. (2001), Climate variability and the influence of the Sun, *Science*, *294*, 2109–2111.
Haigh, J. D. (2007), The Sun and the Earth's climate, *Liv. Rev. Sol. Phys.*, http://solarphysics.livingreviews.org/Articles/lrsp-2007-2/.
Hansen, J. E. (2000), The Sun's role in long-term climate change, *Space Sci. Rev.*, *94*, 349–356.
Harder, J. W., J. M. Fontenla, P. Pilewskie, E. C. Richard, and T. N. Woods (2009), Trends in solar spectral irradiance variability in the visible and infrared, *Geophys. Res. Lett.*, *36*, L07801, doi:10.1029/2008GL036797.
Harvey, K. L. (1992), The cyclic behavior of solar activity, in *ASP Conf. Ser. 27: The Solar Cycle*, pp. 335–367.
Harvey, K. L. (1993), Magnetic dipoles on the Sun, Ph.D. thesis, Univ. of Utrecht Utrechet, Netherlands.
Harvey, K. L. (1994), The solar magnetic cycle, in *Solar Surface Magnetism*, edited by R. J. Rutten and C. J. Schrijver, p. 347, Kluwer, Dordrecht, Netherlands.
Hoyt, D. V., and K. H. Schatten (1993), A discussion of plausible solar irradiance variations, 1700–1992, *J. Geophys. Res.*, *98*, 18,895–18,906, doi:10.1029/93JA01944.
Ikhsanov, R. N., and V. G. Ivanov (1999), Properties of space and time distribution of solar coronal holes, *Solar Phys.*, *188*, 245–258.
Krivova, N. A., and S. K. Solanki (2004), Effect of spatial resolution on estimating the Sun's magnetic flux, *Astron. Astrophys.*, *417*, 1125–1132.
Krivova, N. A., S. K. Solanki, M. Fligge, and Y. C. Unruh (2003), Reconstruction of solar total and spectral irradiance variations in cycle 23: is solar surface magnetism the cause?, *Astron. Astrophys.*, *399*, L1–L4.
Krivova, N. A., S. K. Solanki, and L. Floyd (2006), Reconstruction of solar UV irradiance in cycle 23, *Astron. Astrophys.*, *452*, 631–639.
Krivova, N. A., L. Balmaceda, and S. K. Solanki (2007), Reconstruction of solar total irradiance since 1700 from the surface magnetic flux, *Astron. Astrophys.*, *467*, 335–346.
Krivova, N. A., S. K. Solanki, T. Wenzler, and B. Podlipnik (2009a), Reconstruction of solar UV irradiance since 1974, *J. Geophys. Res.*, *114*, D00I04, doi:10.1029/2009JD012375.
Krivova, N. A., S. K. Solanki, and T. Wenzler (2009b), ACRIM-gap and total solar irradiance revisited: Is there a secular trend between 1986 and 1996?, *Geophys. Res. Lett.*, *36*, L20101, doi:10.1029/2009GL040707.
Krivova, N. A., S. K. Solanki, and Y. C. Unruh (2010), Towards a long-term record of solar total and spectral irradiance, *J. Atm. Sol.-Terr. Phys.*, in press, doi:10.1016/j.jastp.2009.11.013.
Kurucz, R. (1993), ATLAS9 Stellar Atmosphere Programs and 2 km/s grid., *ATLAS9 Stellar Atmosphere Programs and 2 km/s grid. Kurucz CD-ROM No. 13*, Smithsonian Astrophysical Observatory, Cambridge, MA.
Kurucz, R. L. (2005), ATLAS12, SYNTHE, ATLAS9, WIDTH9, et cetera, *Mem. Soc. Astron. It. Suppl.*, *8*, 14–24.
Langematz, U., K. Matthes, and J. L. Grenfell (2005), Solar impact on climate: modeling the coupling between the middle and the lower atmosphere, *Mem. Soc. Astron. It.*, *76*, 868–875.
Lean, J. (2000), Evolution of the Sun's spectral irradiance since the Maunder minimum, *Geophys. Res. Lett.*, *27*, 2425–2428, doi:10.1029/2000GL000043.
Lean, J., G. Rottman, J. Harder, and G. Kopp (2005), SORCE contributions to new understanding of global change and solar variability, *Solar Phys.*, *230*, 27–53, doi:10.1007/s11207-005-1527-2.
Lockwood, M. (2005), Solar outputs, their variations and their effects on Earth, in *The Sun, Solar Analogs and the Climate, 34th 'Saas Fee' Advanced Course*, edited by I. Rüedi, M. Güdel, and W. Schmutz, pp. 109–306, Springer, Berlin.
Lockwood, M., A. P. Rouillard, and I. D. Finch (2009), The rise and fall of open solar flux during the current grand solar maximum, *Astrophys. J.*, *700*, 937–944, doi:10.1088/0004-637X/700/2/937.
Preminger, D. G., and S. R. Walton (2005), A new model of total solar irradiance based on sunspot areas, *Geophys. Res. Lett.*, *32*, L14109, doi:10.1029/2005GL022839.
Schrijver, C. J., and K. L. Harvey (1994), The photospheric magnetic flux budget, *Solar Phys.*, *150*, 1–18.
Solanki, S. K. (2003), Sunspots: An overview, *Astron. Astroph. Rev.*, *11*, 153–286.
Solanki, S. K., M. Schüssler, and M. Fligge (2000), Evolution of the Sun's large-scale magnetic field since the Maunder minimum, *Nature*, *408*, 445–447.
Solanki, S. K., M. Schüssler, and M. Fligge (2002), Secular variation of the Sun's magnetic flux, *Astron. Astrophys.*, *383*, 706–712.
Solanki, S. K., N. A. Krivova, and T. Wenzler (2005), Irradiance models, *Adv. Space Res.*, *35*, 376–383.
Solomon, S., D. Qin, M. Manning, Z. Chen, M. Marquis, K. B. Averyt, M. Tignor, and H. L. Miller (Eds.) (2007), *Climate Change 2007: The Physical Science Basis. Contribution of Working Group I to the Fourth Assessment Report of the Intergovernmental Panel on Climate Change*, Cambridge Univ. Press, Cambridge, U. K., and New York.
Steinhilber, F., J. Beer, and C. Fröhlich (2009), Total solar irradiance during the Holocene, *Geophys. Res. Lett.*, *36*, L19704, doi:10.1029/2009GL040142.
Tran, T., L. Bertello, R. K. Ulrich, and S. Evans (2005), Magnetic fields from SOHO MDI converted to the Mount Wilson 150 foot solar tower scale, *Astrophys. J. Suppl. Ser.*, *156*, 295–310, doi:10.1086/426713.
Unruh, Y. C., S. K. Solanki, and M. Fligge (1999), The spectral dependence of facular contrast and solar irradiance variations, *Astron. Astrophys.*, *345*, 635–642.
Unruh, Y. C., N. A. Krivova, S. K. Solanki, J. W. Harder, and G. Kopp (2008), Spectral irradiance variations: Comparison between observations and the SATIRE model on solar rotation time scales, *Astron. Astrophys.*, *486*, 311–323.
Usoskin, I. G., S. K. Solanki, C. Taricco, N. Bhandari, and G. A. Kovaltsov (2006), Long-term solar activity reconstructions: Direct test by cosmogenic ^{44}Ti in meteorites, *Astron. Astrophys.*, *457*, L25–L28.
Vieira, L. E. A., and S. K. Solanki (2010), Evolution of the solar magnetic flux on time scales of years to millenia, *Astron. Astrophys.*, *509*, A100, doi:10.1051/0004-6361/200913276.
Wang, Y.-M., J. L. Lean, and N. R. Sheeley (2005), Modeling the Sun's magnetic field and irradiance since 1713, *Astrophys. J.*, *625*, 522–538, doi:10.1086/429689.
Wenzler, T. (2005), Reconstruction of solar irradiance variations in cycles 21–23 based on surface magnetic fields, Ph.D. thesis, ETH Zürich.
Wenzler, T., S. K. Solanki, N. A. Krivova, and C. Fröhlich (2006), Reconstruction of solar irradiance variations in cycles 21–23 based on surface magnetic fields, *Astron. Astrophys.*, *460*, 583–595.
Woods, T. N., W. K. Tobiska, G. J. Rottman, and J. R. Worden (2000), Improved solar Lyman-α rradiance modeling from 1947 through 1999 based on UARS observations, *J. Geophys. Res.*, *105*(A12), 27,195–27,215, doi:10.1029/2000JA000051.

N. A. Krivova and S. K. Solanki, Max-Planck-Institut für Sonnensystemforschung, Max-Planck-Str. 2, D-37191 Katlenburg-Lindau, Germany. (natalie@mps.mpg.de)

L. E. A. Vieira, Laboratory for Physics and Chemistry of the Terrestrial Environment, CNRS, F-45071 Orléans CEDEX 2, France.